J Solid State Electrochem (2002) 6: 217–224
DOI 10.1007/s100080100231

ORIGINAL PAPER

Maxim Y. Avdeev · Mikhail V. Patrakeev
Vladislav V. Kharton · Jorge R. Frade

Oxygen vacancy formation and ionic transport in $Sr_4Fe_6O_{13\pm\delta}$

Received: 7 May 2001 / Accepted: 12 June 2001 / Published online: 16 August 2001

Abstract Oxygen permeation through dense $Sr_4Fe_6O_{13\pm\delta}$ membranes was found to be limited by the bulk ambipolar conductivity. At 1173 K and oxygen partial pressures 10 to 1.01×10^5 Pa, ionic conductivity of intergrowth strontium ferrite increases with reducing oxygen pressure, indicating that the vacancy migration mechanism provides a greater contribution to ionic transport in comparison with the interstitial diffusion. The ion transference numbers of $Sr_4Fe_6O_{13\pm\delta}$ increase from 2.5×10^{-4} to 1.9×10^{-3} when the oxygen pressure decreases. Combined X-ray and neutron powder diffraction studies of oxygen-deficient $Sr_4Fe_6O_{13-\delta}$ showed an accumulation of oxygen vacancies in the non-perovskite layers, built of oxygen-iron polyhedra with pentacoordinated Fe cations. Both thermal and chemically-induced expansion of $Sr_4Fe_6O_{13\pm\delta}$ lattice have pronounced anisotropic character and are considerably lower than that typical for perovskite-type strontium ferrite. The average thermal expansion coefficients of $Sr_4Fe_6O_{13\pm\delta}$ ceramics at 770–1100 K in oxidizing and reducing atmospheres vary in the range $(10.8–13.2)\times10^{-6}$ K^{-1}.

Keywords Strontium ferrite · Neutron diffraction · Oxygen permeation · Oxygen vacancy · Ionic conductivity

Introduction

Layered perovskite-related phases based on $Sr_4Fe_6O_{13\pm\delta}$ compound are receiving considerable attention due to possible applications in ceramic membranes for oxygen separation and partial oxidation of light hydrocarbons [1, 2, 3, 4, 5, 6, 7, 8, 9, 10, 11, 12, 13, 14]. The first works by Balachandran et al. have reported unusually high oxygen permeability and an improved stability of $Sr_4Fe_4Co_2O_x$ ceramics ([1, 2, 3, 4] and references therein). However, more detailed studies [5, 6, 7, 8, 9, 10] showed phase decomposition of Co-containing materials on heating and at reduced oxygen pressures; the permeation fluxes through dense $Sr_4(Fe,Co)_6O_x$ membranes [6, 7, 8] are found significantly less compared to the first works [1, 2]. The mechanism of oxygen ionic conduction in $Sr_4Fe_6O_{13\pm\delta}$-based phases, discussed in numerous papers [4, 5, 7, 10, 11], is still unclear. As a rule, a combination of oxygen vacancy migration and interstitial diffusion is assumed [4, 10, 11], with the concentrations of oxygen interstitials and vacancies related by the Frenkel-type equilibrium. The oxygen hyperstoichiometry of $Sr_4Fe_6O_{13+\delta}$ under oxidizing conditions is as high as $\delta = 0.41$ at room temperature [5] and vary in the range 0.05–0.15 at $p(O_2) = 21–101$ kPa and $T = 1173–1273$ K [11, 12], suggesting possible significant contribution of interstitial oxygen to the ionic transport.

The crystal structure of $Sr_4Fe_6O_{13\pm\delta}$ phase, prepared for the first time by Kanamaru et al. [15], is orthorhombic and can be described using Ibam or Iba2 space groups; the latter space group provides better refinement [16]. This structure consists of perovskite-type layers alternated by slabs of five-coordinated iron polyhedra (Fig. 1). Three non-equivalent sites of iron atoms were found, one octahedral and two five-coordinated positions: trigonal bipyramidal and square pyramidal [16]. Migration of ion charge carriers, both oxygen vacancies and interstitials, was assumed to occur in the layer formed by the pyramids and bipyramids along the a–c plane, whereas the perovskite layers formed by the octahedra act as the frame in the lattice [4, 5].

The present work, focused on studying structure and ionic conductivity of $Sr_4Fe_6O_{13\pm\delta}$ as functions of oxygen content, represents a continuation of our research on ionic transport in oxide materials based on

M.Y. Avdeev · M.V. Patrakeev · V.V. Kharton (✉) · J.R. Frade
Department of Ceramics and Glass Engineering, UIMC,
University of Aveiro, 3810–193 Aveiro, Portugal
E-mail: kharton@cv.ua.pt

M.V. Patrakeev
Institute of Solid State Chemistry, Ural Division of RAS,
91 Pervomaiskaya Str., Ekaterinburg 620219, Russia

V.V. Kharton
Institute of Physicochemical Problems, Belarus State University,
14 Leningradskaya Str., 220080 Minsk, Republic of Belarus

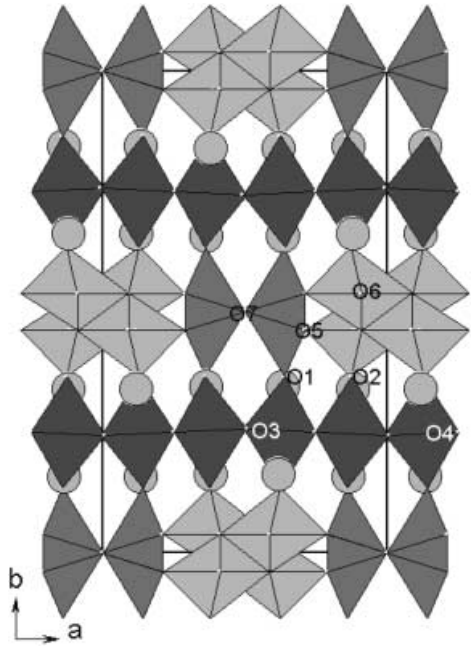

Fig. 1 View of $Sr_4Fe_6O_{13+\delta}$ structure along the c axis. The *circles* correspond to Sr cations; oxygen anions are located at the corners of FeO_x polyhedra

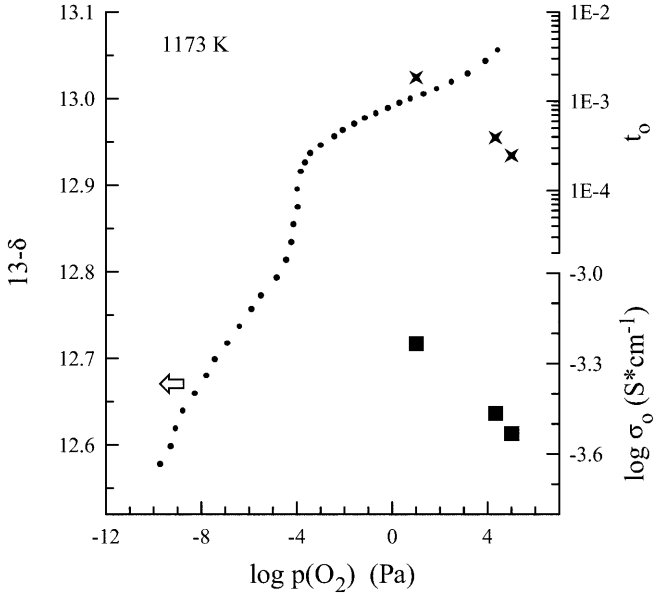

Fig. 2 Oxygen partial pressure dependencies of the oxygen nonstoichiometry, oxygen ionic conductivity, and ion transference numbers of $Sr_4Fe_6O_{13\pm\delta}$ at 1173 K

the Sr-Fe-O system [12, 14, 17, 18, 19, 20]. As an attempt to reveal positions of oxygen vacancies and, possibly, interstitials, the structural studies were performed using a combination of X-ray and neutron powder diffraction. More detailed data on oxygen nonstoichiometry and total conductivity of $Sr_4Fe_6O_{13\pm\delta}$ were published elsewhere [12].

Experimental

Single-phase $Sr_4Fe_6O_{13\pm\delta}$ powder was prepared by a standard ceramic route using high-purity $SrCO_3$ and Fe_2O_3 as starting materials, in the stoichiometric proportion. The solid-state reaction was conducted at 1220–1420 K for 40 h in air with multiple intermediate regrindings. After X-ray diffraction (XRD) analysis demonstrated formation of the single phase, selected portions of the powder were annealed in different atmospheres in order to prepare samples with various oxygen content for structural studies. The first of them, hereafter referred to as "oxidized", was annealed at 1173 K for 8 h in pure oxygen flow and then slowly cooled under the same conditions. The second sample was annealed at 1173 K in a flow of argon (oxygen partial pressure of approximately 1 Pa) for 8 h, and then cooled in a closed chamber. According to the data on oxygen nonstoichiometry of $Sr_4Fe_6O_{13\pm\delta}$ (Fig. 2), such treatment allows one to obtain approximately stoichiometric material. Finally, the "reduced" sample was annealed at 1173 K in a flow of N_2-H_2 mixture (oxygen partial pressure of 10^{-12} Pa) for 20 h; the total oxygen content in this case is expected close to 12.55 (Fig. 2 and [12]).

For preparation of dense $Sr_4Fe_6O_{13\pm\delta}$ ceramics, the stoichiometric mixture of starting materials was dissolved in an aqueous solution of nitric acid, dried, and then thermally decomposed. Single-phase powder, obtained after the reaction at 1170–1370 K for 25 h in air with several regrindings, was ball-milled and then pressed at 250–350 MPa in the shape of disks of various thickness (diameter 10–20 mm). Gas-tight ceramics were sintered in air at 1470–1490 K for 6–10 h. After sintering, the samples were annealed in air at 1170 K for 5–6 h with subsequent slow cooling. XRD confirmed that the ceramics was single phase. For the ceramic samples, the unit cell parameters calculated from the XRD data were very similar to those of as-prepared powder, subjected to treatments in various gas atmospheres prior to structural studies. The density of the ceramic samples was higher than 92% of their theoretical density.

X-ray powder diffraction data were collected at room temperature using Rigaku D/Max-B diffractometer (CuK_γ radiation, 2Θ angle range from 8 to 108°, step 0.02°, 10 s/step). Neutron powder diffraction experiments have been carried out at room temperature and at 3 K using the high-resolution G4.2 (LLB, France) diffractometer (wavelength 2.3434, $2\Theta = 3$–172, step 0.1, total measuring time for each sample 14 h). Rietveld refinements of combined X-ray and neutron data were performed with multi-pattern version of the Fullprof program [21].

The prepared materials were characterized using scanning electron microscopy and energy dispersive spectroscopy (SEM/EDS), emission spectroscopic analysis, dilatometry, measurements of electrical conductivity, oxygen permeability, and Faradaic efficiency. Detailed description of the experimental procedures and equipment used for the characterization was published elsewhere ([12, 14, 17, 18, 19, 20, 22] and references therein). The data on oxygen nonstoichiometry (Fig. 2) were obtained using coulometric titration and thermal gravimetric analysis (TGA); the details are found in [12].

In this paper, the oxygen permeation processes are analyzed using the quantities of the permeation flux density j ($mol \times s^{-1} \times cm^{-2}$), and specific oxygen permeability $J(O_2)$ ($mol \times s^{-1} \times cm^{-1}$) defined as [23]

$$J(O_2) = j \cdot d \cdot \left[\ln \frac{p_2}{p_1}\right]^{-1} \quad (1)$$

where d is the membrane thickness, and p_1 and p_2 are the oxygen partial pressures at the membrane permeate and feed sides, respectively ($p_1 < p_2$). Using the quantity $J(O_2)$ is convenient to identify a limiting effect of the surface exchange rate on the permeation, on the basis of the thickness dependence of the permeation flux [18, 22]. Since this quantity is proportional to j×d by definition, the specific oxygen permeability should be independent of thickness in the case when surface limitations to the oxygen

permeation flux are negligible. In such a situation, $J(O_2)$ is proportional to the ambipolar conductivity (σ_{amb}) of the membrane material, averaged for a given oxygen partial pressure range:

$$J(O_2)=\frac{RT}{16F^2}\cdot\overline{\sigma_{amb}}=\frac{RT}{16F^2}\cdot\overline{\frac{\sigma_o\cdot\sigma_e}{\sigma_o+\sigma_e}}=\frac{RT}{16F^2}\cdot\overline{\sigma\cdot t_o(1-t_o)} \quad (2)$$

where t_o is the oxygen ion transference number, and σ, σ_o, and σ_e are the total, oxygen ionic, and electronic conductivities, respectively. When oxygen exchange limitations are considerable, $J(O_2)$ should increase with increasing membrane thickness due to a decreasing role of the surface exchange, for a given oxygen chemical potential gradient.

Results and discussion

Structure

Selected results of the structural refinement of $Sr_4Fe_6O_{13\pm\delta}$ are presented in Fig. 3 and in Tables 1 and 2. As a starting model, X-ray single crystal data on the $Sr_4Fe_6O_{13}$ phase, presumably stoichiometric [16], were used. The coordinates of all atoms and occupancies of oxygen sites were refined while the thermal parameters were fixed to the values found by Yoshiasa et al. [16] in order to avoid strong correlation with other parameters and to increase the reflections/parameters ratio.

The powder diffraction patterns were analyzed in order to detect possible presence of other phases of Sr-Fe-O system, including $SrFeO_3$, $SrFeO_{2.5}$, $SrFe_{12}O_{19}$, $SrFe_2O_5$, etc. No phase impurities were found; both powders and ceramics of $Sr_4Fe_6O_{13\pm\delta}$ were single phase. The presence of traces of $SrFe_{12}O_{19}$ observed by Bredesen et al. [11] in undoped $Sr_4Fe_6O_{13\pm\delta}$ ceramics might thus be due to their synthesis route.

The neutron diffraction data on the isostructural phase, $Sr_4Fe_4Co_2O_x$, were recently reported by Mitchell et al. [9, 24], who observed the reflections defying I-centering conditions of Iba2 group. In this study, no reflections related to violation of the conditions hkl ($h+k+l=2n$), h0l ($h=2n$), 0kl ($k=2n$) have been found. As the Neel temperature of $Sr_4Fe_6O_{13}$ compound is 418 ± 5 K [15], the magnetic peaks appear at low angles in neutron diffraction pattern. Their intensity increases with decreasing temperature (Fig. 4), which makes it possible to distinguish these reflections from structure peaks. Due to the small number of non-overlapping reflections, the magnetic cell could not be indexed; the region containing the strongest magnetic peaks was thus excluded from the refinement. However, remaining magnetic peaks overlap with the structure reflections and decrease the quality of the refinement in the case of neutron diffraction data (Fig. 3).

Two methods were used to identify the location of hyperstoichiometric oxygen in oxidized $Sr_4Fe_6O_{13+\delta}$: the difference Fourier maps analysis and the analysis of the voids in the structure. The most suitable void was found near Fe2 position having square pyramidal coordination; this hypothetical site completes the coordination of iron ion to distorted octahedral. However, the refinement did not converge to any reasonable results, indicating either the distribution of oxygen over several sites with a weak occupation or the dynamic character of the excess oxygen disorder.

In contrast, the refinement of the data on reduced $Sr_4Fe_6O_{13-\delta}$ allowed to determine unambiguously the location of oxygen vacancies. Reduction of intergrowth strontium ferrite was found to decrease the occupancies of O5, O6, O7 sites only (0.88(2), 0.95(2), 0.90(2) respectively). These sites are located in the slab built of five-coordinated iron polyhedra (Fig. 1). Such an accumulation of the vacancies reflects the tendency to decreasing the coordination number and, probably, switching to distorted tetrahedral coordination.

Thermal and chemically-induced expansion

The unit cell constants obtained from the refinement exhibit a reasonable behavior on cooling (Tables 1 and 3). The parameter b, which is perpendicular to the perovskite layers (Fig. 1), provides the most significant contribution in the cell contraction, the behavior typical for layered structures (for example, [25, 26]). Reduction of $Sr_4Fe_6O_{13\pm\delta}$ leads to longer b, while the a and c parameters decrease with decreasing oxygen content (Table 1). Again, this phenomenon is characteristic of layered perovskite-related phases [25, 26], where the chemically-induced expansion on reduction is, as a rule, maximum for the axis perpendicular to the perovskite-type layers. Due to the lattice contraction along the perovskite planes, average chemically-induced expansion of the intergrowth compounds is considerably smaller with respect to perovskite phases [25]. In particular, the values of the volume thermal expansion coefficients (TECs) of the reduced and oxidized $Sr_4Fe_6O_{13\pm\delta}$ are very similar (Table 3). Notice that the volume TECs (β) are related to the linear thermal expansion coefficients as $\beta\approx\alpha_a+\alpha_b+\alpha_c$; in case of average linear TEC (α), this approximate ratio is $\beta\approx3\alpha$. It should also be mentioned that the reduction of strontium ferrite is accompanied by increasing the distance between apical oxygen ions sited in octahedra of the perovskite-type layer; this may suggest that Fe^{2+} cations formed due to decreasing oxygen content are mainly located in the perovskite slabs.

At higher temperatures, variation in oxygen content in $Sr_4Fe_6O_{13\pm\delta}$ ceramics results in a greater difference of thermal expansion coefficients (Table 4). In particular, changing the atmosphere from atmospheric air to N_2-H_2 mixture leads to an increase in the average TEC from 10.8×10^{-6} to 13.2×10^{-6} K^{-1}. The higher thermal expansion in reducing atmosphere is obviously related to the higher oxygen vacancy concentration (for instance, [27]). Nevertheless, the TECs of $Sr_4Fe_6O_{13\pm\delta}$ are considerably lower than that of perovskite-type phases based on $SrFeO_{3-\delta}$ [19, 20]. This is in agreement with the observation [25] that increasing the ratio between perovskite and non-perovskite layers in intergrowth perovskite-related compounds increases their thermal expansion.

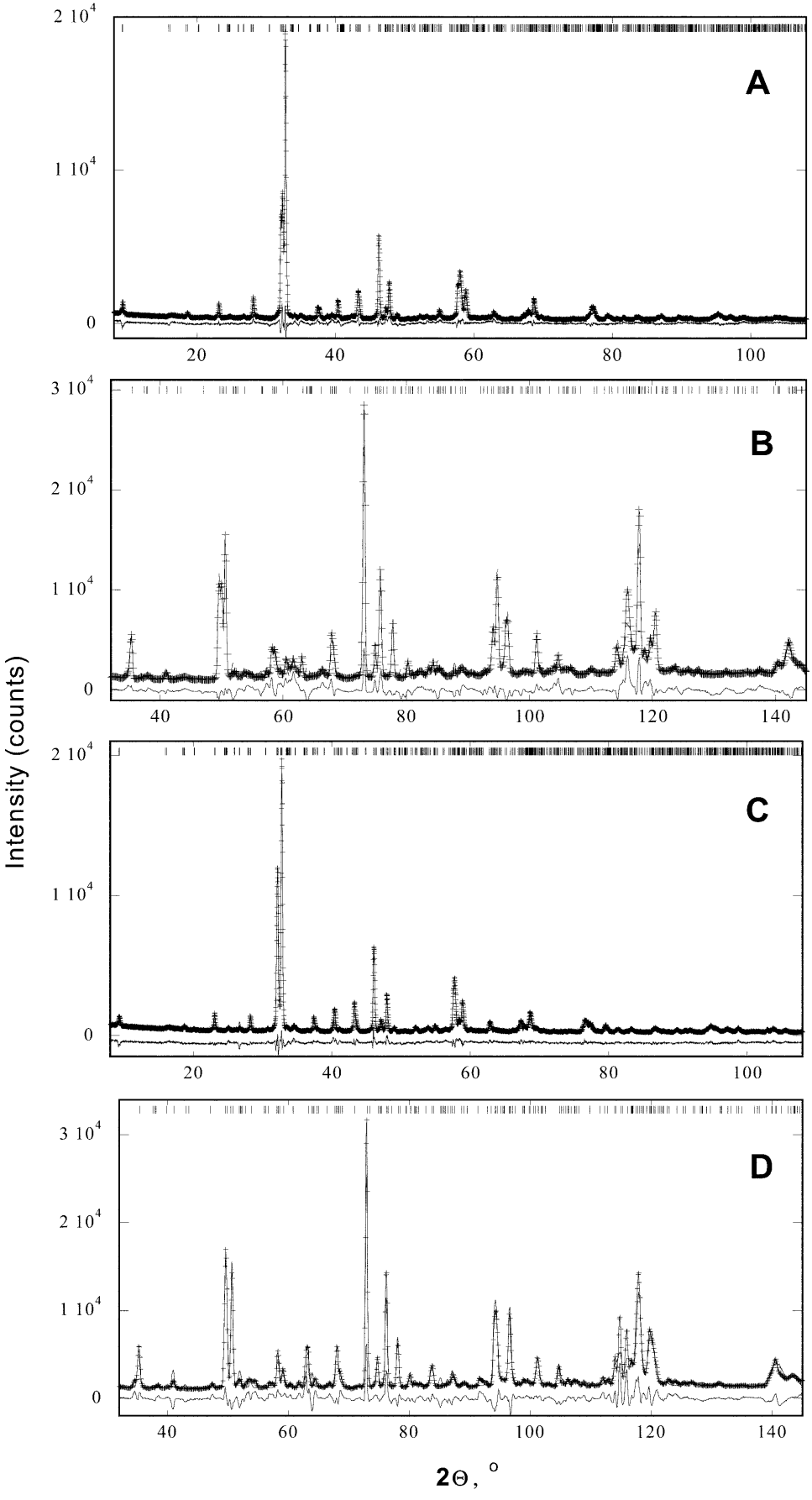

Fig. 3A–D Observed, calculated, and difference: **A,C** X-ray; **B,D** neutron diffraction patterns of the reduced (*top*) and oxidized $Sr_4Fe_6O_{13\pm\delta}$

Table 1 The results of structural refinement of $Sr_4Fe_6O_{13\pm\delta}$, annealed in different atmospheres

Treatment atmosphere	Lattice parameters, Å						Volume, $Å_3$	
	a		b		c		295 K	3 K
	295 K	3 K	295 K	3 K	295 K	3 K		
O_2	11.167(1)	11.146(2)	18.976(1)	18.916(2)	5.5597(7)	5.5514(9)	1178.1(2)	1170.4(2)
Ar	11.155(2)		18.903(2)		5.5516(9)		1170.6(2)	
N_2+H_2	11.1516(6)	11.134(1)	19.052(1)	18.994(2)	5.5310(3)	5.5200(5)	1175.1(3)	1167.4(2)

Space group Iba2 (45); Z = 4; R_p (O_2, 295 K) = 0.12; R_{wp} (O_2, 295 K) = 0.16; R_p (N_2+H_2, 295 K) = 0.13; R_{wp} (N_2+H_2, 295 K) = 0.17

Table 2 Fractional atomic coordinated in reduced and oxidized $Sr_4Fe_6O_{13\pm\delta}$ at room temperature

Atom	Reduced			Oxidized		
	x	y	z	x	y	z
Sr1	0.3717(17)	0.3390(9)	0.7955(5)	0.3754(11)	0.3418(9)	0.9230(5)
Sr2	0.3740(19)	0.1565(8)	0.7835(4)	0.3650(10)	0.1588(9)	0.9167(5)
Fe1	0.1305(14)	0.0404(10)	0.7997(4)	0.1281(14)	0.0385(11)	0.9639(5)
Fe2	0.1186(11)	0.4563(11)	0.8109(4)	0.1316(14)	0.4528(14)	0.0068(4)
Fe3	0.1241(17)	0.2465(11)	0.7996(6)	0.1241(13)	0.2519(12)	0.9406(4)
O1	0.139(3)	0.134(2)	0.802(2)	0.120(5)	0.135(2)	0.934(2)
O2	0.125(3)	0.362(2)	0.783(1)	0.124(4)	0.360(2)	0.931(1)
O3	0.003(4)	0.250(3)	0.059(1)	0.005(4)	0.249(3)	0.171(2)
O4	0.248(4)	0.251(3)	0.056(1)	0.250(6)	0.250(3)	0.183(2)
O5	0.204(3)	0.032(2)	0.160(3)	0.210(6)	0.029(2)	0.273(3)
O6	0.423(3)	0.045(2)	0.679(3)	0.423(7)	0.040(2)	0.857(3)
O7	0.5	0.5	0.533(3)	0.5	0.5	0.750(3)

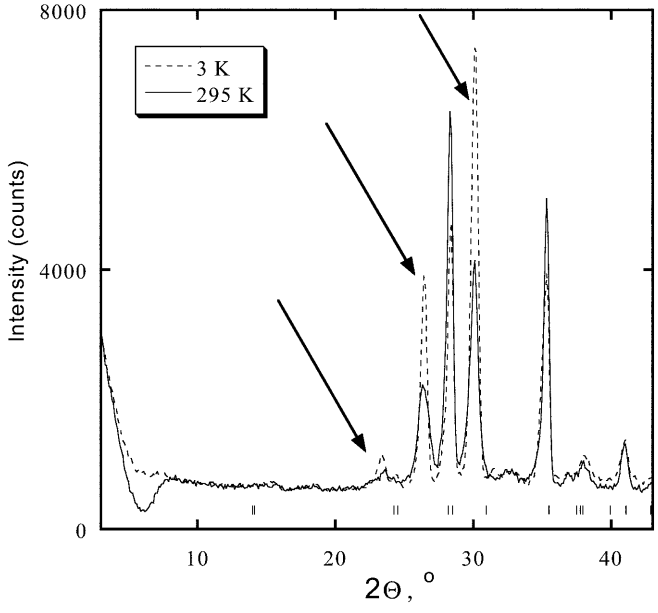

Fig. 4 The increase in the extra peaks intensity on cooling along with the constant intensity of structure peaks, indicating their magnetic nature

Table 3 Average thermal expansion coefficients (TECs) of $Sr_4Fe_6O_{13\pm\delta}$ at 3–295 K, estimated from the neutron diffraction data

Material	$\alpha_a\times10^6$, K^{-1}	$\alpha_b\times10^6$, K^{-1}	$\alpha_c\times10^6$, K^{-1}	$\beta\times10^6$, K^{-1}
Reduced	5.4	10.5	6.8	22.6
Oxidized	6.4	10.9	5.1	22.5

α_a, α_b are α_c are the coefficients of linear thermal expansion along a, b and c axes, respectively. β is the coefficient of volume thermal expansion, related to the average linear TEC by the approximate ratio $\beta = 3\alpha$

Table 4 Average thermal expansion coefficients of $Sr_4Fe_6O_{13\pm\delta}$ at 770-1100 K, estimated from the dilatometric data

Atmosphere	$\alpha\times10^6$, K^{-1}
Air	10.8 ± 0.2
N_2	11.4 ± 0.4
N_2+H_2 (2% H_2)	13.2 ± 0.3

Oxygen permeability

Figure 5A shows the dependencies of steady oxygen permeation fluxes through two $Sr_4Fe_6O_{13\pm\delta}$ membranes with different thickness on the oxygen chemical potential gradient; the corresponding values of the specific oxygen permeability are given in Fig. 5B. It should be noted that the obtained permeation fluxes are quite close to the data of Manthiram et al. [7, 8]. The difference between $J(O_2)$ values is insignificant within the experimental error limits (Fig. 5B), suggesting that the integral form of the Wagner equation is observed and the effect of the surface exchange on permeation is negligible. Thus, when the membrane thickness is higher than 0.6 mm, the oxygen transport through $Sr_4Fe_6O_{13\pm\delta}$ ceramics membranes is limited by the bulk ambipolar conductivity.

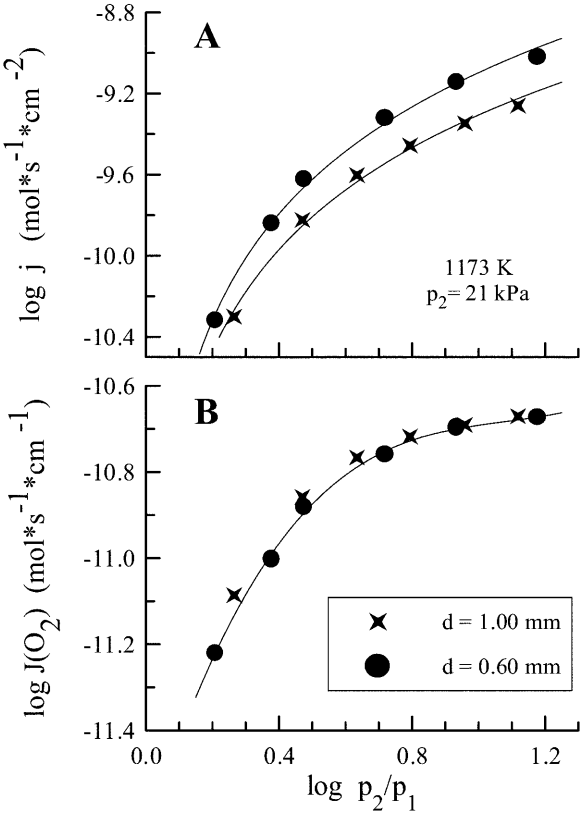

Fig. 5A,B Dependence of: **A** the oxygen permeation flux density; **B** specific oxygen permeability of $Sr_4Fe_6O_{13\pm\delta}$ membranes on the oxygen partial pressure gradient at 1173 K

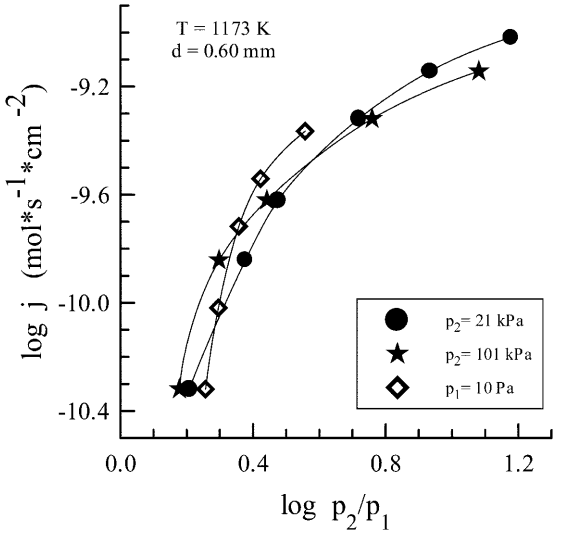

Fig. 6 Dependence of the oxygen permeation flux density through $Sr_4Fe_6O_{13\pm\delta}$ membrane on the oxygen partial pressure gradient at 1173 K and fixed permeate-side or feed-side oxygen pressure

$$\overline{\sigma_{amb}} = \frac{(4F)^2 d}{RT} \cdot \left(\frac{\partial j}{\partial \ln(p_2/p_1)}\right)_{\ln\left[\frac{p_2}{p_1}\right]\to 0} \tag{3}$$

$$t_o = \frac{1}{2} - \frac{1}{2}\sqrt{1 - 4\frac{\overline{\sigma_{amb}}}{\sigma}} \tag{4}$$

This makes it possible to calculate the ion transference numbers and ionic conductivity from the permeation and total conductivity data (Eq. 2).

Figure 6 presents the data on oxygen permeability at several oxygen partial pressures, fixed at the membrane feed or permeate side. The curves in Fig. 6 are related to the same driving force for the oxygen transport, expressed as $\log(p_2/p_1)$; the observed variations in the permeation fluxes are therefore caused by the changes of the ambipolar conductivity. When the oxygen pressure gradients are large enough, oxygen permeation and ambipolar conductivity both increase with decreasing average oxygen chemical potential. At small driving forces, greater permeability is observed at higher $p(O_2)$ values. However, in the latter case the observed behavior may partially result from the experimental error associated with extremely small values of the permeation fluxes. In particular, one possible reason for such phenomena could be related to a pseudo-steady oxygen desorption by the sample, which may act as an oxygen capacity.

Ionic conductivity

Calculation of ion transference numbers (t_o) from the permeation and total conductivity data was carried out using the relationships (see Eq. 2)

The total conductivity values used for the calculations are listed in Table 5; detailed data on the total conductivity of $Sr_4Fe_6O_{13\pm\delta}$ as a function of oxygen pressure are found elsewhere [12]. For the calculations, only the oxygen permeation data corresponding to the values of $\log(p_2/p_1)$ less than 0.5 were selected.

The ion transference numbers and oxygen ionic conductivity of $Sr_4Fe_6O_{13\pm\delta}$ at 1173 K are presented in Fig. 2. The ionic conductivity increases with reducing oxygen pressure, indicating that, for the studied $p(O_2)$ range, the vacancy migration mechanism provides a greater contribution to ionic transport. This behavior and the decrease of p-type electronic conductivity, typical for $Sr_4Fe_6O_{13\pm\delta}$ in oxidizing conditions [12], result in the increase of the ion transference numbers from 2.5×10^{-4} to 1.9×10^{-3} when the oxygen pressure decreases from 1.01×10^5 to 10 Pa. The transference numbers obtained in this work are considerably less with

Table 5 Total electrical conductivity of $Sr_4Fe_6O_{13\pm\delta}$ at 1173 K at various oxygen partial pressures

$p(O_2)$, Pa	σ, S/cm
1.01×10^5	1.19
2.1×10^4 Pa	0.87
10.1	0.32
1×10^{-7}	2.88

respect to the data by Ma and Balachandran [4] on $Sr_4Fe_4Co_2O_x$ ceramics, for which the t_o values in air were reported as high as 0.4–0.5 at 870–1270 K. However, the results of Faradaic efficiency tests confirmed that the oxygen ion transference numbers of $Sr_4Fe_6O_{13\pm\delta}$ do not exceed 2×10^{-3}. Also, the e.m.f. of oxygen concentration cells with $Sr_4Fe_6O_{13\pm\delta}$ membranes was found negligible, suggesting a very low ionic contribution to the total conductivity.

Final comments

The neutron diffraction studies of oxygen-deficient $Sr_4Fe_6O_{13-\delta}$ showed that oxygen vacancies are located in the $Fe_2O_{2.5-\delta}$ layers consisting of iron-oxygen pohyhedra where the iron cations have distorted tetragonal pyramidal and trigonal bipyramidal coordination; the perovskite layer consisting of FeO_6 octahedra remains essentially unchanged under variations of oxygen pressure. Therewith, the contribution of oxygen vacancy migration to the total ionic transport seems to be predominant, at least, at oxygen pressures below 10^5 Pa. In contrast to disordered perovskite-type phases, the diffusion by the vacancy mechanism in the lattice of $Sr_4Fe_6O_{13\pm\delta}$ should be anisotropic; structural consideration of the diffusion pathways allows one to expect a faster transport along the c axis. In addition, contrary to disordered perovskites, only part of the lattice oxygen takes part in the ionic conduction. These factors as well as a random grain orientation in $Sr_4Fe_6O_{13\pm\delta}$ ceramics result in the very low ionic conductivity of intergrowth strontium ferrite.

Another necessary comment is that the obtained results show a predominant role of the vacancy migration mechanism in the ionic transport at $p(O_2) \le 10^5$ Pa, but an increase in the oxygen pressure may cause a greater role of the oxygen interstitial diffusion. Indeed, under the small oxygen chemical potential gradients, oxygen permeation flux through $Sr_4Fe_6O_{13-\delta}$ membrane at $p_2 = 1.01\times10^5$ Pa is higher than that at $p_2 = 2.1\times10^4$ Pa (Fig. 6). In both these cases, further increase in the driving force is associated with lower average oxygen chemical potential gradient along the membrane, when the contribution of the vacancy mechanism increases. Hence, more detailed studies of ionic transport at $p(O_2) > 10^5$ Pa should be performed in order to reveal the role of oxygen interstitials.

Finally, the $Sr_4Fe_6O_{13\pm\delta}$ phase is stable over a wide range of oxygen partial pressures and exhibits relatively low thermal expansion, which might be of interest for high-temperature electrochemical devices. However, both ionic and electronic conductivities of $Sr_4Fe_6O_{13\pm\delta}$ are low. The oxygen permeability of $Sr_4Fe_6O_{13\pm\delta}$ ceramics is less with respect to the most permeable $SrFeO_{3-\delta}$- and $SrCoO_{3-\delta}$-based materials by 10^2–10^4 times (for instance [18, 19, 20]). Therefore, application of $Sr_4Fe_6O_{13\pm\delta}$ in high-temperature electrochemical cells without appropriate modifications is very problematic. One possible method to enhance the ionic conductivity may refer to texturing of the ceramic material in order to achieve preferential grain orientation.

Conclusions

Single-phase intergrowth strontium ferrite $Sr_4Fe_6O_{13\pm\delta}$ was prepared by standard ceramic synthesis technique. Oxygen-deficient, approximately stoichiometric and oxygen hyperstoichiometric $Sr_4Fe_6O_{13\pm\delta}$ samples were obtained by thermal treatments in different atmospheres and studied by X-ray and neutron powder diffraction. For oxygen-deficient $Sr_4Fe_6O_{13-\delta}$, oxygen vacancies were found to be located in the non-perovskite layers consisting of oxygen-iron tetragonal pyramids and trigonal bipyramids. On reduction, the unit cell parameter perpendicular to the perovskite layers increases, whilst two others decrease. Thermal expansion of both reduced and hyperstoichiometric $Sr_4Fe_6O_{13\pm\delta}$ has pronounced anisotropic character. This results in a moderate chemically-induced and thermal expansion of $Sr_4Fe_6O_{13\pm\delta}$ lattice as compared to the perovskite-type strontium ferrite. The thermal expansion coefficients of $Sr_4Fe_6O_{13\pm\delta}$ ceramics at 770–1100 K, calculated from the dilatometric data in oxidizing and reducing atmospheres, vary in the range $(10.8–13.2)\times10^{-6}$ K^{-1}. Oxygen permeation through dense $Sr_4Fe_6O_{13\pm\delta}$ membranes with thickness higher than 0.6 mm is limited by the bulk ambipolar conductivity. At 1173 K and oxygen partial pressures from 10 to 1.01×10^5 Pa, ionic conduction in the intergrowth strontium ferrite increases with reducing oxygen pressure, indicating that the vacancy migration mechanism provides a greater contribution to ionic transport in comparison with oxygen interstitial diffusion. The ion transference numbers increase from 2.5×10^{-4} to 1.9×10^{-3} when the oxygen pressure decreases from 1×10^5 to 10 Pa.

Acknowledgements Partial financial support of this work has been provided by the FCT, Portugal (Praxis program and the contract P/CTM/14170/98), and the Russian Foundation for Basic Research (grant 01–03–96519). The experiment at LLB was supported by the European Commission through the Access to Research Infrastructures action of the Improving Human Potential Programme (contract HPRI–CT–1999–00032). The authors are sincerely grateful to Dr. A. Kurbakov (LLB) for his help with neutron data collection and useful discussions, and to Dr. B. Mitchell (Argonne National Laboratory) for preprints of his publications.

References

1. Balachandran U, Kleefisch MS, Kobylinski TP, Morissette SL, Pei S (1994) Int Patent Application PCT WO 94/24065
2. Balachandran U, Ma B, Maiya PS, Mieville RL, Dusek JT, Picciolo JJ, Guan J, Dorris SE, Liu M (1998) Solid State Ionics 108:363
3. Ma B, Balachandran U, Hodges JP, Jorgensen JD, Miller DJ, Richardson JW (1998) Mater Lett 35:303
4. Ma B, Balachandran U (1997) Solid State Ionics 100:53

5. Guggilla S, Manthiram A (1997) J Electrochem Soc 144:L120
6. Kim S, Yang YL, Christoffersen R, Jacobson AJ (1998) Solid State Ionics 109:187
7. Armstrong T, Prado F, Xia Y, Manthiram A (2000) J Electrochem Soc 147:435
8. Xia Y, Armstrong T, Prado F, Manthiram A (2000) Solid State Ionics 130:81
9. Mitchell BJ, Richardson JW, Murphy CD, Ma B, Balachandran U, Hodges JP, Jorgensen JD (2000) Mater Res Bull 35:491
10. Bredesen R, Norby T (2000) Solid State Ionics 129:285
11. Bredesen R, Norby T, Bardal A, Lynum V (2000) Solid State Ionics 135:687
12. Patrakeev MV, Mitberg EB, Leonidov IA, Kozhevnikov VL (2001) Solid State Ionics 139:325
13. Ran S, Zhang X, Yang PH, Jiang M, Peng DK, Chen CS (2000) Solid State Ionics 135:681
14. Kozhevnikov VL, Leonidov IA, Patrakeev MV, Mitberg EB, Poeppelmeier KR (2001) J Solid State Chem (accepted)
15. Kanamaru F, Shimada M, Kiozumi M (1972) J Phys Chem Solids 33:1169
16. Yoshiasa A, Ueno K, Kanamaru F, Horiuchi H (1986) Mater Res Bull 21:175
17. Leonidov IA, Kozhevnikov VL, Mitberg EB, Patrakeev MV, Kharton VV, Marques FMB (2001) J Mater Chem 11:1202
18. Kharton VV, Tikhonovich VN, Shuangbao L, Naumovich EN, Kovalevsky AV, Viskup AP, Bashmakov IA, Yaremchenko AA (1998) J Electrochem Soc 145:1363
19. Kharton VV, Kovalevsky AV, Viskup AP, Jurado JR, Figueiredo FM, Naumovich EN, Frade JR (2001) J Solid State Chem 156:437
20. Kharton VV, Viskup AP, Kovalevsky AV, Jurado JR, Naumovich EN, Vecher AA, Frade JR (2000) Solid State Ionics 133:57
21. Rodriguez-Carvajal J (1993) Physica B 192:55
22. Kovalevsky AV, Kharton VV, Tikhonovich VN, Naumovich EN, Tonoyan AA, Reut OP, Boginsky LS (1998) Mater Sci Eng B 52:105
23. Moebius H-H (1986) Oxygen current density coefficient of oxidic materials. In: Extended Abstracts 37th Meeting ISE, vol. 1. Vilnius, Lithuania, pp 136–139
24. Mitchell BJ, Richardson JW, Murphy CD, Ma B, Balachandran U, Hodges JP, Jorgensen JD (2000) J Europ Ceram Soc (in press)
25. Vashook VV (2000) DSc Thesis, Belarus Academy of Sciences, Minsk, Belarus (in Russian)
26. Mizusaki J, Tagawa H, Hayakawa K, Hirano K (1995) J Am Ceram Soc 78:1781
27. Hayashi H, Suzuki M, Inaba H (2000) Solid State Ionics 128:131